Co-Activation Patterns in Neonates using High-Density Diffuse Optical Tomography: Insights into Early Dynamic Functional Connectivity

K. Lee[a], T. Austin[a], J. Uchitel[a], C. Caballero-Gaudes[b,c], L. Collins-Jones[d], R. Cooper[e], A. Edwards[f], J. Hebden[e], G. Kromm[d], K. Pammenter[f], B. Blanco[g]

[a] *Department of Paediatrics, University of Cambridge, Cambridge, UK*

[b] *Basque Center on Cognition Brain and Language (BCBL), Donostia-San Sebastián, Spain*

[c] *Ikerbasque, Basque Foundation for Science, Bilbao, Spain*

[d] *Department of Clinical Neurosciences, University of Cambridge, Cambridge, UK*

[e] *Department of Medical Physics and Biomedical Engineering, University College London, London, UK*

[f] *Cambridge University Hospitals NHS Foundation Trust, Cambridge, UK*

[g] *Department of Psychology, University of Cambridge, Cambridge, UK*

Abstract

Dynamic functional connectivity (FC) in neonates is a growing area of interest due to the developmental significance of early functional networks. There are several emerging techniques to measure dynamic FC, adding new perspectives to well-studied static FC networks. Recent dynamic FC studies suggest that adult resting state networks are driven by key moments of dynamic activity rather than sustained correlations. Co-activation pattern (CAP) analysis leverages this theory, clustering high-activity frames to identify recurring configurations of significant activity. High-density diffuse optical tomography (HD-DOT) is an infant-friendly modality that measures hemodynamic changes in the cortex. HD-DOT has been used to investigate static FC in term-aged infants. The CAP approach is a promising avenue to examine dynamic FC in neonates, but it is yet untested in neonatal HD-DOT. This study validates the CAP approach for neonatal HD-DOT and presents novel decompositions of neonate FC networks.

HD-DOT data were acquired from a cohort of sleeping term newborns at the Rosie Hospital, Cambridge UK (n = 44, postmenstrual age = 40+3 (range: 38+2 - 42+6) weeks). The top 15% of seed-selected frames were clustered using the K-means algorithm for three regions of interest (ROIs: frontal, central, and parietal) to identify significant seed-associated patterns of co-activation or co-deactivation. These patterns (CAPs) were characterized using four metrics: consistency, fractional occupancy, dwell time, and transition likelihood.

Distinct CAPs were identified for frontal, central, and parietal regions of interest. These CAPs had high consistency scores, validating the efficacy of the CAP methodology for newborn HD-DOT. The CAP decomposition revealed significant patterns obscured by static analysis. Several neonate CAPs illustrate frontoparietal activity, potentially reflecting early default mode network activity, which is immature and modular for the first year after birth.

This work demonstrates the utility of CAP analysis with newborn HD-DOT and provides new insight into brain dynamics of early resting state networks.

1. Introduction and Background

The first year after birth is marked by significant functional changes in the human brain (Keunen et al., 2017; Stoecklein et al., 2020). Studying functional maturation in the neonatal period is critical for characterizing patterns of typical and atypical brain development and their association with lifelong neurodevelopmental variation. Despite the critical importance of understanding early brain development, there is a paucity of neonatal brain studies when compared with the prevalence of adult brain imaging research, resulting in promising novel methods developed for adults that remain untested in neonatal populations. This disparity potentially stems from the challenging nature of imaging the newborn brain due to the unique needs—both technological and analytical—of neonatal participants (Mohammadi-Nejad et al., 2018).

Although functional magnetic resonance imaging (fMRI) has greatly advanced our knowledge of early brain development and is generally regarded as the gold standard for functional neonatal brain imaging, fMRI is not particularly suited to neonatal studies (Edwards et al., 2022; Eyre et al., 2021; Keunen et al., 2017). fMRI requires motion-free scans, and neonates (asleep or awake) move frequently and unpredictably (Arthurs et al., 2012; Mohammadi-Nejad et al., 2018). It is for this reason that neonates used to be sedated before fMRI scans, which was suboptimal as sedation has been found to modulate brain activity (Gemma et al., 2009; Hassanzadeh et al., 2023; Keunen et al., 2017; Mohammadi-Nejad et al., 2018). Despite advances in protocols for scanning awake infants (Deen et al., 2017), fMRI is not conducive to naturalistic studies as neonates are scanned in a loud machine isolated from their mothers, disrupting their natural environment (Arthurs et al., 2012; Mohammadi-Nejad et al., 2018). Wearable high-density diffuse optical tomography (HD-DOT) systems have been recently developed to facilitate infant studies owing to their comfortable design, relatively increased resilience to motion artifacts, and cot-side applicability (C. W. Lee et al., 2017; Uchitel et al., 2023). HD-DOT is a functional near-infrared spectroscopy (fNIRS) technology that uses an array of overlapping multi-distance sources and detectors to map the concentration of oxygenated hemoglobin ([HbO]) and deoxygenated hemoglobin ([HbR]) in three-dimensions of the cortex. HD-DOT can image changes in [HbO] and [HbR] with higher temporal resolution than fMRI and superior spatial resolution compared to electroencephalography (EEG), though, like EEG, it is limited to cortical imaging (Peng & Hou, 2021; Uchitel et al., 2023). These features of wearable HD-DOT have permitted studies of newborn infant functional connectivity (Uchitel et al., 2023).

Functional connectivity is a keystone concept in mapping typical and atypical brain development, quantifying the operative relationship between disparate regions of the brain. Specifically, it refers to the strength of the covariance or correlation of activity between brain regions over time (Power et al., 2010). Though functionally connected brain regions may be spatially remote, they are temporally coupled (Arimitsu et al., 2022). Functional brain networks are groups of functionally related regions and are associated with certain neurophysiological events (Menon, 2013; Power et al., 2010). fMRI has been used to reliably detect several resting-state networks in adult brains (e.g., default-mode network, primary sensorimotor network, visual network, and language network) (M. H. Lee et al., 2013; J. Yang et al., 2020). Although much remains unknown about the emergence of these networks, several fMRI

studies have explored functional connectivity in the infant brain. From birth, primary sensorimotor and visual networks are present, and throughout the first year, additional networks gradually emerge, starting with primary networks and later followed by higher-order networks (Gao et al., 2017). By age one, several resting state networks resemble their analogous adult networks, including primary and secondary visual networks, dorsal attention, and default mode network. Still, some networks are underdeveloped by age one, such as the frontoparietal executive control network (Gao et al., 2017).

These studies provide important insight into early brain development. However, they approach functional connectivity from the conventional "static" point of view. "Static functional connectivity" refers to the average functional connectivity over the course of the data collection window. This traditional approach is robust but does not capture the time-varying components of functional connectivity in the brain, which is naturally non-stationary. Dynamic functional connectivity studies aim to describe functional interactions between brain regions that fluctuate over time, adding depth and accuracy to our understanding of the brain (Hutchison et al., 2013; Preti et al., 2017). In recent years, many fMRI, EEG, and fNIRS studies have explored methods to measure functional connectivity dynamically in order to paint a more nuanced and accurate depiction of brain activity. Several groups have explored different measures of dynamic functional connectivity such as neural flexibility, temporal variability, and stability of correlation coefficients (Hutchison et al., 2013; Preti et al., 2017; Wen et al., 2020; Yin et al., 2020). Notably, these dynamic features of functional connectivity change with age (Qin et al., 2015) and can be used to differentiate adult controls from patients diagnosed with schizophrenia (Shen et al., 2014) or Alzheimer's disease (Jones et al., 2012). This dynamic approach is particularly promising for neonatal studies, where data is often fragmented due to motion artifacts or short scanning sessions.

In contrast to static functional connectivity measures like seed-based correlation or independent component analysis (ICA), which require clean and continuous data segments, dynamic functional connectivity analysis operates on a finer time scale and is therefore more tolerant of fragmented datasets. This flexibility makes it a promising approach for neonatal studies, which often encounter motion artifacts or are limited to short scanning sessions. Several groups have investigated neonatal dynamic functional connectivity, dynamically characterizing resting-state networks in term and preterm neonates. Their methods vary, drawing upon analogous adult studies in the fMRI community. Three neonatal studies calculate dynamic functional connectivity using a sliding-window approach, temporally partitioning the BOLD signal into overlapping or non-overlapping segments and then calculating parcel or voxel correlation matrices in these windows (Niu et al., 2020; Ren et al., 2022; Wang et al., 2024). Another popular approach is to window ICA time courses and identify significant patterns of network interactions using clustering algorithms like K-means (López-Vicente et al., 2021; Ma et al., 2020; Marusak et al., 2017).

These frameworks extract dominant connectivity patterns at the group level and quantify how they vary over time. As with many window-based analyses, this method is sensitive to changes in analysis parameters such as window and step length which cannot be empirically chosen (Cabral et al., 2017; Hutchison et al., 2013). To address the issue

of parameter sensitivity, a new analysis methodology was developed for fMRI data that does not depend on time-domain parameters (Liu & Duyn, 2013b). This method revealed that resting-state brain activity is driven by distinct, instantaneous brain configurations occurring at single time points. These configurations, which repeat over time, are referred to as co-activation patterns (CAPs) and can be identified using unsupervised clustering techniques. The CAPs' spatial configurations describe significant arrangements of instantaneous brain activity, and the CAPs' metrics, such as dwell time and fractional occupancy, describe the dynamic features of the patterns. The premise of CAP analysis conceptually and procedurally resembles that of EEG microstate studies. Microstate analysis has been used successfully in neonate and infant resting state EEG studies to identify similarities between adult and infant microstates and to study global brain dynamics in preterm neonates (Brown & Gartstein, 2023; Hermans et al., 2023). So far, CAPs and CAP metrics have been used in a variety of experimental conditions to examine task, state, and cohort differences in adult and pediatric populations; however, they have not been applied to neonatal populations (Adhikari et al., 2021; Marshall et al., 2020; Mawla et al., 2023; H. Yang et al., 2021).

So far, CAP analysis in HD-DOT has been limited (Khan et al., 2022), and, to the best of our knowledge, CAP analysis has not been applied to HD-DOT neonate data. This study has two objectives: first, to validate CAP analysis for neonatal HD-DOT; second, to shed light on early dynamic functional connectivity by presenting the first HD-DOT CAP decomposition of task-free neonatal networks in term-aged neonates.

2.0 Methods

2.1 Participants

The National Research Ethics Service East of England Committee approved this study (REC reference 15/LO/0358). Written informed consent was provided by the parents of 82 healthy newborn infants (born ≥ 37 weeks' gestation) at Rosie Hospital (Cambridge University Hospitals NHS Foundation Trust). 38 neonates were excluded from the study post-data collection due to insufficient quantity of motion-free data (see Section 2.3), consistent with the exclusion rate typically observed in fNIRS infant studies (C. W. Lee et al., 2017; Uchitel et al., 2023). Data from 44 neonates were preprocessed and analyzed (n female = 15; median gestational age [GA] = 40+0 (range: 38+1 - 42+1) weeks; median postmenstrual age [PMA] = 40+3 (range: 38+2 - 42+6) weeks; median age at time of study = 2 (range: 0 - 11) days; median birth weight = 3.405 (range: 2.415 - 4.240) kg; median head circumference = 34.5 (range: 33.0 - 37.0) cm. 28 of the 44 neonatal datasets were utilized by Uchitel et al., which examined static functional connectivity (Uchitel et al., 2023).

2.2 Data Collection

HD-DOT data were collected cot-side using a modular wearable HD-DOT technology called LUMO (Gowerlabs Ltd, UK, https://www.gowerlabs.co.uk/). Gowerlabs assisted in the construction of LUMO caps customized for two neonatal head circumferences (34 cm and 36 cm). These caps were fitted with 12 HD-DOT tiles, each containing 3 sources and 4 detectors (36 sources and 48 detectors in total), and were designed to cover frontal, central, and

parietal regions of interest (ROI). The neonatal LUMO caps were capable of collecting intensity data for two wavelengths (735 nm and 850 nm) at a sampling rate of 10 Hz.

Data collection followed the protocol outlined previously (Uchitel et al., 2023). Neonates were recorded while sleeping in their cot on the postnatal ward. Parents were typically present throughout the duration of the study. If the infant was restless, they were swaddled and/or fed to encourage sleep. Though data were ideally collected for an hour or more, some studies were terminated early due to the infant waking up, wanting to feed, or encountering immediate clinical procedures. Synchronized video of the infant was captured to confirm the neonate remained asleep during acquisition. Lastly, a 3D scan of the infant's head was collected using the "Scandy Pro" iPhone application (Scandy LLC, USA) for digitization of head landmarks and tile locations. These locations were used to scale the neonatal head model for image reconstruction.

2.3 HD-DOT Data Preprocessing

Data preprocessing for this study was based on the framework used in a previous HD-DOT infant study (Uchitel et al., 2023), with modifications to better suit the current study objectives. All preprocessing was done in MATLAB R2021b (Mathworks, USA) using a mixture of original scripts and the following fNIRS MATLAB toolboxes: Homer2 (Huppert et al., 2009) and DOT-HUB (https://github.com/DOT-HUB). Motion-free data segments (duration ≥ 100 seconds) were extracted from each participant's dataset using the *hmrMotionArtifact* function from Homer2, an fNIRS data analysis toolbox, and concatenated. Participants with less than three minutes of concatenated motion-free data were excluded from further analysis. Channels were evaluated using a sliding window approach (window = 33% the length of the segment, overlap = 50%) and were removed if their coefficient of variation exceeded 12 or if their average signal was outside our range of interest (1e-4 ≤ mean signal ≤ 2.5). Data were converted from optical density to [HbO] and [HbR] using the *hmrConc2OD* function from the Homer2 toolbox. Following methods described in previous studies (Sato et al., 2016), non-neuronal hemodynamic sources of noise such as scalp-hemodynamics were regressed out of the concentration data using short separation regression, a process which regresses out the average of short distance channels (<10 mm) activity to attenuate scalp-level physiological confounds. Attenuating physiological confounds increases the likelihood of obtaining measures from cerebral rather than extra-cerebral origin (Yücel et al., 2021). Temporal filtering was performed in a linear regression model. Contributions of high-frequency physiological noise sources such as respiration and cardiac pulsation were accounted for in the model by including Fourier terms for frequencies above 0.08 Hz (Blanco et al., 2021). Slow frequency fluctuations and signal drifts were also accounted for in the model by adding the kth order Legendre polynomials (where k = 1 + floor(duration in seconds / 150)) because their spectral power predominantly consists of very low frequencies. Concentration data was converted back to optical density using the *hmrConc2OD* function from the Homer2 toolbox. Lastly, since hemodynamic changes in the brain happen on the scale of seconds, the data was downsampled to 1 Hz to reduce computational load of data processing.

2.4 HbO and HbR Image reconstruction

Photogrammetry software called CloudCompare (https://www.cloudcompare.org/) was utilized to calculate the relative locations of each source, detector, and neonatal head landmarks in the Scandy Pro head scans. Next, an affine transformation (computed using head landmarks positions) was used to register the source and detector coordinates to an infant head model (*DOTHUB_LUMO2NIRS* function from the DOTHUB toolbox). This model was sourced from a neonatal head model database and was selected based on the average head circumference of the cohort (Collins-Jones et al., 2021).

Images of brain activity were reconstructed according to the procedure outlined by Uchitel et al. which employs the DOTHUB and Toast++ MATLAB toolboxes (Schweiger & Arridge, 2014; Uchitel et al., 2023). The Jacobian matrix (calculated using Toast++ toolbox) was first constructed to be 30 x 30 x 30 voxels and then projected into a 3D infant-specific head mesh. To model [HbO] and [HbR] concentration, tissue absorption at wavelengths 735 and 850 nm were specifically modeled. Changes in absorption coefficients at these wavelengths were calculated by inverting the zeroth-order forward model (calculated using diffusion approximation) (Arridge, 1999; Arridge & Schotland, 2009). These relative absorption coefficient differentials were used to create images of changes in [HbO] and [HbR]. Images were mapped from the volume mesh (626580 nodes) to the surface mesh (34194 nodes) of the head model for cortical visualization.

A group-level sensitivity mask was calculated by finding the sensitivity for each surface node at the participant level using the *DOTHUB_MakeGMSensitivityMap* function. A node was considered sensitive if it exhibited a sensitivity greater than 10% the maximum value of the normalized Jacobian. A final group-level sensitivity mask was created by identifying nodes to which at least 75% of subjects were sensitive (see Figure 1a).

2.5 Parcellation and Seed Selection

This study aimed to examine brain activity in the three cortical regions covered by the neonatal LUMO system: frontal, parietal, and central regions. These regions were selected to interrogate different and distinct functions (higher executive, somatomotor, and visuospatial processes) which have been well-researched in analogous static functional connectivity studies. Regions were identified using the M-CRIB parcellation scheme, which is a publicly available neonatal head atlas (see Figure 1b) (Alexander et al., 2019). The M-CRIB atlas supplied labels for 9 regions (left and right). Since individual MRI were not available, some M-CRIB parcels were combined to be conservative on resolution. Left and right rostral middle frontal gyrus and superior frontal gyrus labels were combined to create left and right frontal ROI respectively. Left and right precentral gyrus and postcentral gyrus labels were combined to create left and right central ROIs respectively. Left and right superior parietal gyrus and inferior parietal gyrus were combined to create left and right parietal ROIs respectively. In total six ROIs were used in this study (left/right frontal, left/right central, and left/right parietal, see Figure 1c and 1d).

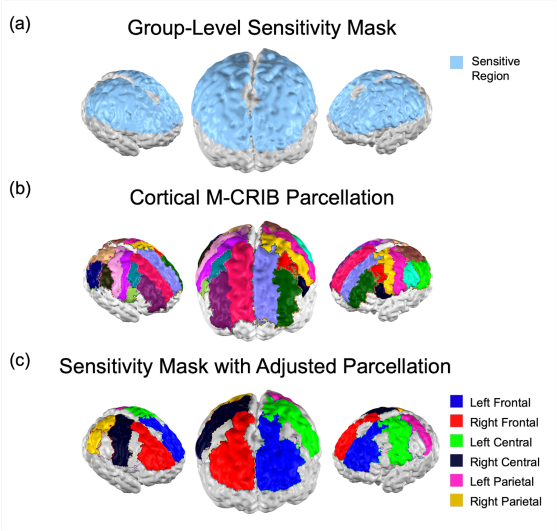

Figure 1. (a) Group-level sensitivity profile coregistered to neonatal head model. (b) M-CRIB parcellation coregistered to the neonatal head model. (c) Group-level sensitivity profile parcellated by M-CRIB labels adjusted for regions of interest.

Since this study relies on seed-based frame selection, it was critical to choose seeds which highlighted activity in the corresponding region of interest. This motivated our decision to calculate optimal seeds at the participant level rather than select a singular seed driven by group-averaged data (see Figure 2b). Candidate seeds were identified by masking out nodes outside the region of interest. Each node in the region served as a candidate seed's center. The candidate seed [HbO] time course was calculated as the mean activity of nodes within 3 mm radius of the seed's center. The candidate seed's time course was correlated with each node in the mesh (excluding nodes that comprised the seed) to create the candidate seed's correlation matrix. A threshold of 0.5 [HbO] was selected to create a binary mask of the correlation matrix. Dice Scores (a measure of similarity) were calculated for each candidate seed's binary correlation matrix and a mask containing the nodes in the region of interest and its bilateral counterpart. The candidate seed with the highest Dice Score is the seed whose activity is best correlated with the nodes in the region of interest. Thus, the candidate seed with the highest Dice Score is labelled the regional seed for that individual. This procedure is repeated for each of the six regions of interest (seed locations are shown in Supplementary Figure 1).

2.6 Frame Selection

In order to examine activity in specific regions, data frames were selected based on seed activity (see Figure 2c). This procedure closely follows Liu and Duyn's pre-clustering procedure for fMRI co-activation pattern analysis (Liu & Duyn, 2013b). Datasets were first z-score normalized within participants to reduce the influence of inter-participant variability. Data frames were sorted by [HbO] activity at the left and right seed locations for a given region of interest. The top 15% of sorted frames for each participant were selected for left and right seeds. This threshold was chosen because the average spatial map of the top 15% of frames is highly correlated with the seed activation map (Figure 3. and Supplementary Figure 2), and gains above this threshold are small, as illustrated by

the figure. This process was used not only to select a threshold, but to validate the CAP procedure against the static approach in this dataset (see Figure 2d). For each ROI, one dataset was created by taking the union of left-seed-selected and right-seed-selected frames.

2.7 K Means Clustering

Since we wanted to take into consideration both [HbO] and [HbR] values from the 10984 sensitive nodes during clustering, we initially had a total of 21968 dimensions (10984 measures of [HbO] and 10984 measures of [HbR], see Figure 2e). Principal Component Analysis (PCA) is a popular dimensionality reduction algorithm used to improve the effectiveness and efficiency of unsupervised machine learning algorithms. PCA is an important preprocessing step for clustering problems with large datasets as it identifies linear combinations of the initial dimensions to reduce variables while retaining overall dataset variance. We used PCA from the Python module *sklearn.decomposition* to PCA transform the group-level data along the node dimension from 21968 nodes to 275 components, retaining 99% of total variance (Pedregosa et al., 2011). This transformation was done independently for each region's dataset (frontal, central, and parietal).

PCA transformed datasets were then clustered using the *KMeans* function from Python's sklearn.cluster module (Pedregosa et al., 2011). K-means is an unsupervised machine learning algorithm which clusters data based on Euclidean distance. First, k centroids are randomly initialized. On each iteration of the algorithm, data points are assigned to their nearest centroid according to Euclidean distance. The centroid locations are then updated to reflect the mean of its associated data points. This step is repeated until the centroids remain stable between iterations (Pedregosa et al., 2011). Data points associated with the same centroid are said to be part of the same "cluster" of data. K-means is usually run several times since clustering results can be sensitive to the random initialization of the centroids. We repeated k-means analysis 100 times using the n_init parameter of sklearn's *KMeans* function, which repeats k-means with different centroid seeds and returns the best run according to centroid inertia. Mean silhouette score, a metric commonly used to quantify cluster separation and similarity, was used to evaluate k-means performance. We tested a range of k (2 - 20) for each region independently and selected the most suitable k using the elbow method (see Supplementary Figure 2). Parameter k = 7 was selected for all three regions.

2.8 Co-Activation Patterns

Each cluster of similar frames corresponds to one CAP. A central CAP containing fewer than 50 frames was excluded from further analysis because the frames appeared to be highly correlated outliers from one participant and was therefore not a generalizable pattern of interest. The clustered frames were averaged together (in node space) to create the final CAP maps, which each have a Δ[HbO] representation and a corresponding Δ[HbR] representation (see Figure 2f).

Following previous CAP and similar clustering studies, we assess CAPs by measuring the consistency, fractional occupancy, dwell time, and transition probability of each CAP (see Figure 2g) (França et al., 2024; Khan et al.,

2022; Liu et al., 2018). CAP consistency refers to the intra-cluster spatial correlation of the CAP and is calculated by finding the mean spatial correlation of the CAP map with each frame in the cluster. Fractional occupancy, also known as occurrence rate or time fraction, is calculated at the participant level and refers to the proportion of frames in the CAP cluster to the total number of frames in the dataset. Dwell time is calculated at the participant level and refers to the mean duration of consecutive frames that belong to the CAP. Transition probability is determined at the participant level and refers to the likelihood of transitioning from CAP X to CAP Y. This is calculated by counting the number of transitions from CAP X to CAP Y and dividing it by the total number of transitions out of CAP X that occur in the dataset.

Though all four metrics characterize the CAPs, achieving high CAP consistency is precursory to further analysis because consistency quantifies how effectively the data was clustered and therefore how meaningful the CAPs are. Low consistency indicates poor data clustering and suggests CAP analysis is not suitable for the dataset. We utilized Liu and Duyn's CAP consistencies (mean ± SD = 0.26 ± 0.04, median = 0.265, range = [0.21, 0.30]) as our benchmark goal in this study and found our CAPs in all regions to have sufficient consistency for further analysis (Liu & Duyn, 2013b). In-participant fractional occupancy, dwell time, and transition probability were calculated for each CAP and averaged across participants.

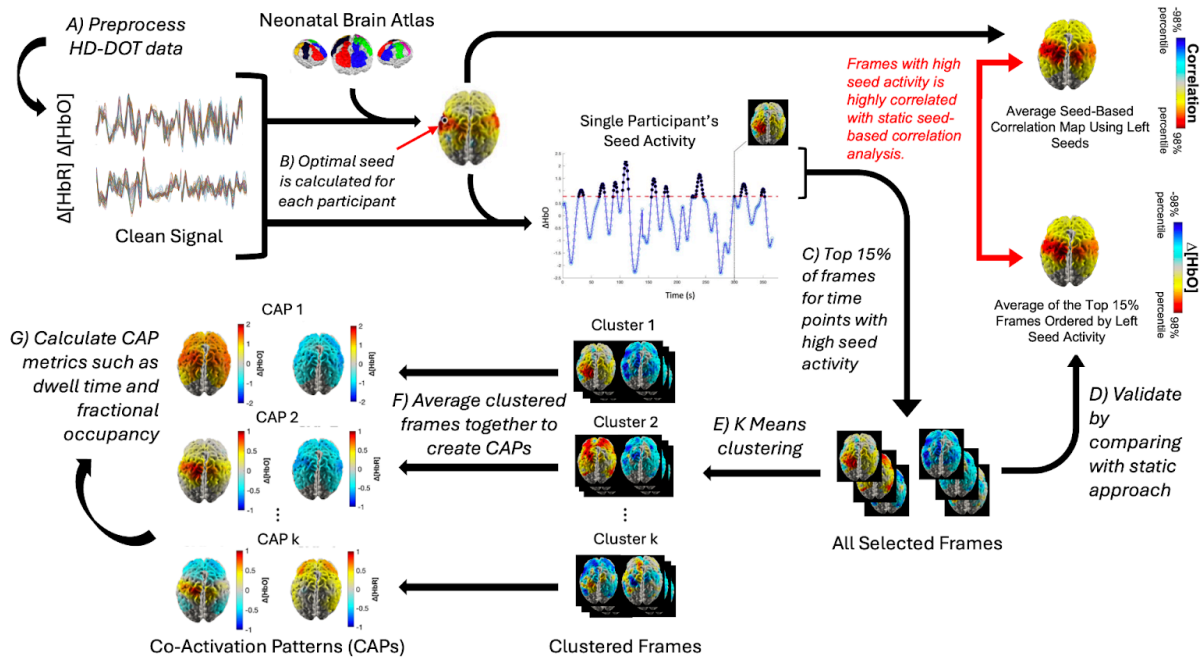

Figure 2. Analysis pipeline from preprocessing to co-activation pattern (CAP) generation.

3.0 Results

3.1 Frame Selection

We verified that the top 15% of frames ordered by seed activity had correlation ≥ 0.95 with the seed-based correlation map for all regions (see Figure 3. and Supplementary Figure 1). The premise for CAP analysis relies on the assumption that some percentage of single time point data frames with high seed activity can substitute for seed-based correlation analysis, a widely used static approach to functional connectivity. As done previously (Liu & Duyn, 2013b), we demonstrate that this assumption holds true for this dataset by verifying that the average of the top 15% frames (ordered by seed activity) is highly correlated to the same seed's correlation map.

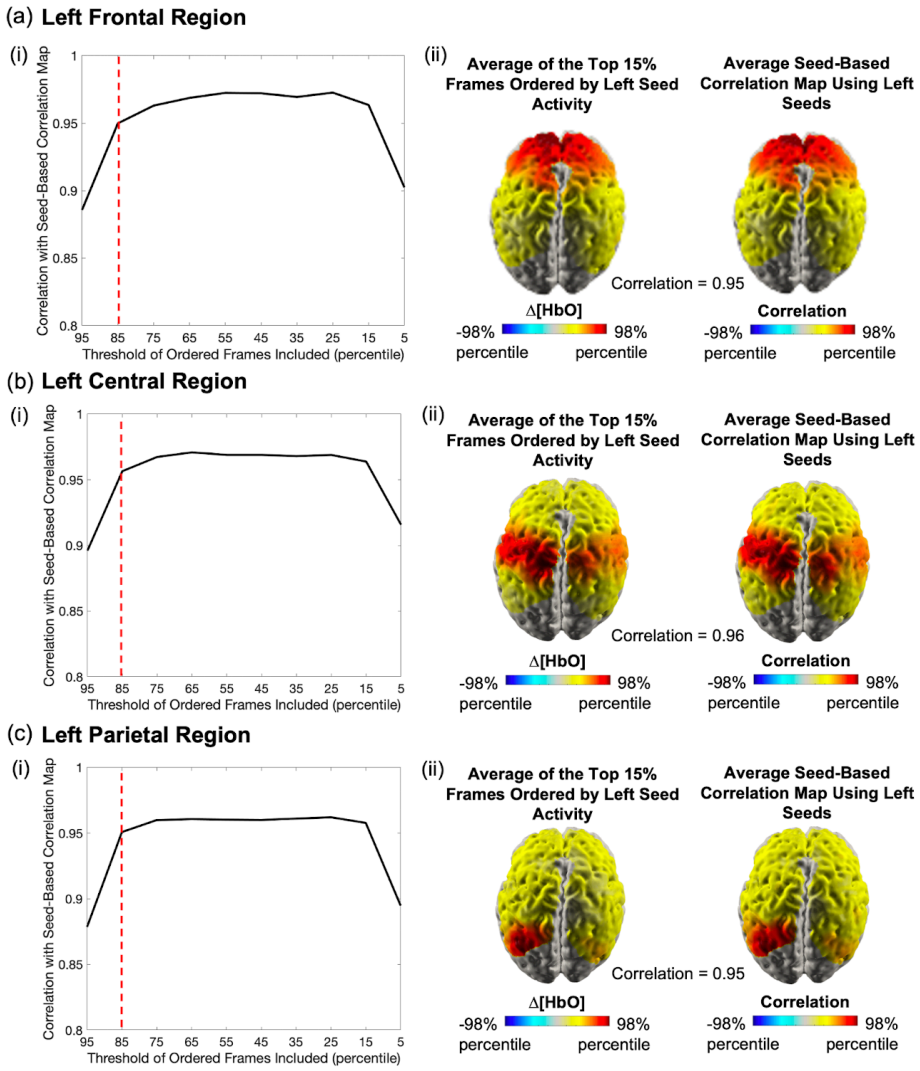

Figure 3. (i) Varying percentile threshold shows top 15% of frames ordered by seed activity is sufficient for high fidelity to static seed-based correlation analysis. (ii) Seed-based correlation maps are highly correlated with the spatial average of the top 15% of HD-DOT frames ordered by seed activity (correlation reported at the bottom of right-side figures). (a) Frontal left region seed analysis. (b) Central left region seed analysis. (c) Parietal left region seed analysis. Right equivalent region available in supplementary material (see Supplementary Figure 2)

3.2 Co-Activation Patterns

The size of the clusters identified through K-means analysis varies within the region (see Supplementary Figure 4). Frames within each cluster were averaged to generate the final CAP maps (see Figure 4 for z-scored [HbO] maps and Supplementary Figure 5 for complementary z-scored [HbR] maps). The CAPs are numbered according to their average consistency, from highest to lowest. Consistency scores were calculated and compared against our benchmark, Liu and Duyn's fMRI CAP study (Liu & Duyn, 2013b). The consistency scores for each region are as follows: Frontal CAPs: mean ± SD = 0.51 ± 0.20, median = 0.53, range = [0.24, 0.82]; Central CAPs: mean ± SD = 0.48 ± 0.22, median = 0.49, range = [0.19, 0.80]; Parietal CAPs: mean ± SD = 0.48 ± 0.21, median = 0.51, range = [0.25, 0.80]. While the mean and median consistency scores in our study exceed the benchmarks set by previous literature, the standard deviation is greater. Despite this, we consider the results satisfactory since each individual CAP's consistency meets or exceeds the thresholds defined in the benchmark study, except for central CAP 6. Although this CAP shows a lower consistency score, it is included to facilitate a complete and transparent report of our analysis. With the exception of this one outlier, the high consistency across the CAPs strongly supports the validity of the identified patterns, justifying further analysis. Figure 5. presents a subset of the CAPs in Figure 4. (frontal CAP 4, parietal CAP 3, parietal CAP 4, parietal CAP 5, and parietal CAP 7) from three views to examine frontoparietal activity.

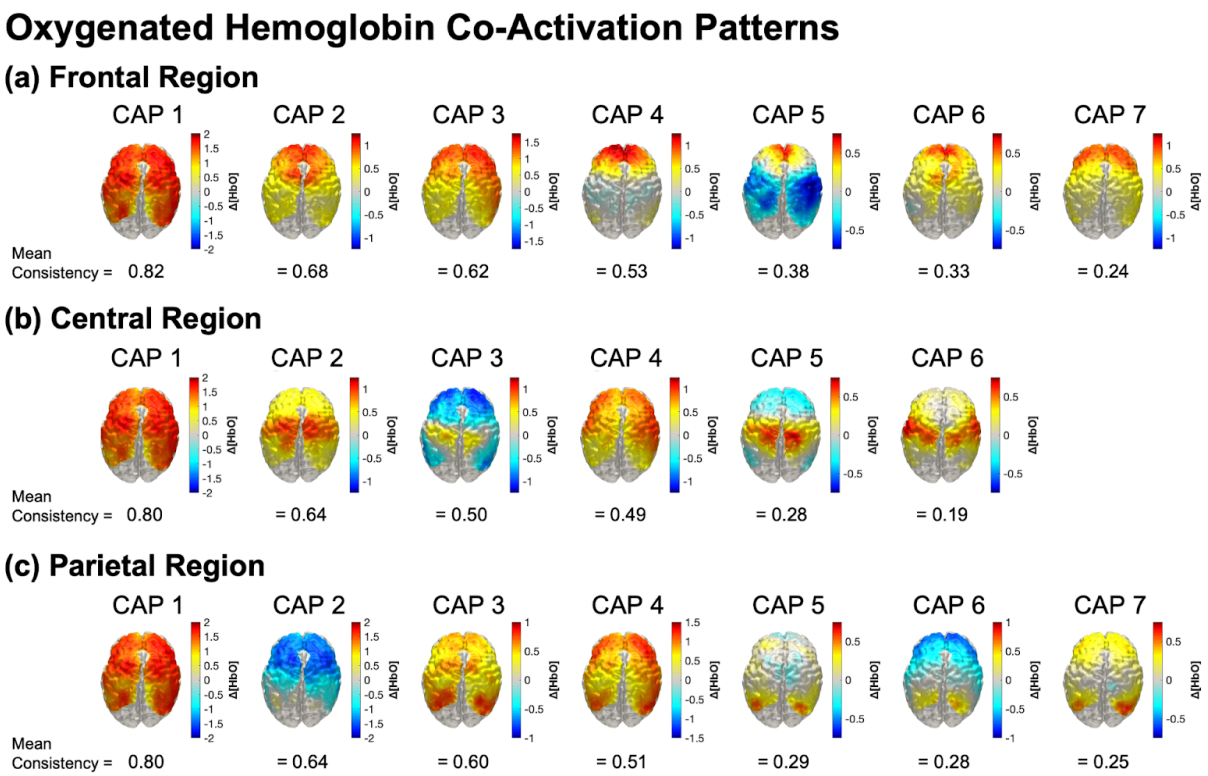

Figure 4. Z-score normalized oxygenated hemoglobin co-activation patterns (CAPs) for (a) frontal, (b) central, and (c) parietal region analyses. From left to right, the CAPs are shown in decreasing order of consistency. Each CAP's deoxygenated hemoglobin counterpart map can be found in the supplementary material (Supplementary Figure 5)

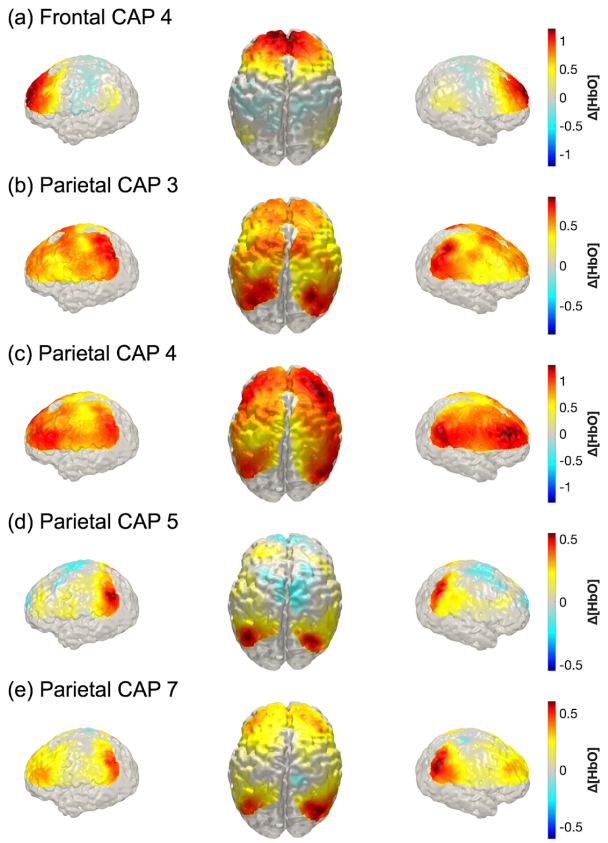

Figure 5. Three views (left lateral, dorsal, and right lateral) of z-score normalized Δ[HbO] co-activation patterns (CAPs) with frontoparietal activity.

3.3 Intra-Participant CAP Metrics

Metrics associated with the temporal features of each CAP, concretely fractional occupancy and dwell time, were explored in this study to check for significant differences within each region (see Supplementary Table 1). All statistical tests were performed in R (R Core Team, 2017). A Shapiro-Wilk test was used to verify normality which was violated in all regions. Since normality was violated, a Friedman test was used to assess whether fractional occupancy and dwell time significantly differed between CAPs within each region while controlling for repeated measures within participants (see Supplementary Table 2). Fractional occupancy was found to be significantly different across CAPs for all three regions ($p = 1.03e-05$, $p = 1.03e-15$, $p = 2.56e-23$ for frontal, central, and parietal regions respectively). Dwell time was also found to be significantly different across CAPs for frontal and central regions (Bonferroni corrected $p = 6.64e-04$ and $p = 5.91e-04$ respectively) but not for the parietal region CAPs (Bonferroni corrected $p = 0.203$). Pairwise differences were evaluated using a paired Wilcoxon test with Bonferroni

correction (corrected for 21 comparisons for frontal and parietal region analyses and 15 comparisons for central region analysis). CAP metrics and significant differences with adjusted p values are shown in Figures 6 and 7.

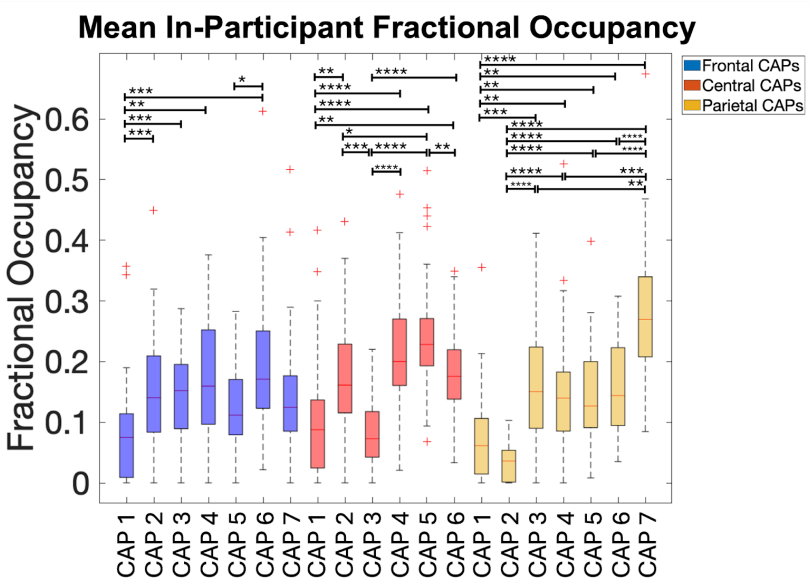

Figure 6. Average in-participant co-activation pattern (CAP) fractional occupancies for all regions of interest. Bracketed pairs show significant statistical differences from Wilcoxon pairwise analysis. Bonferroni corrected: * $p < 0.05$; ** $p < 0.01$; *** $p < 0.001$; **** $p < 0.0001$.

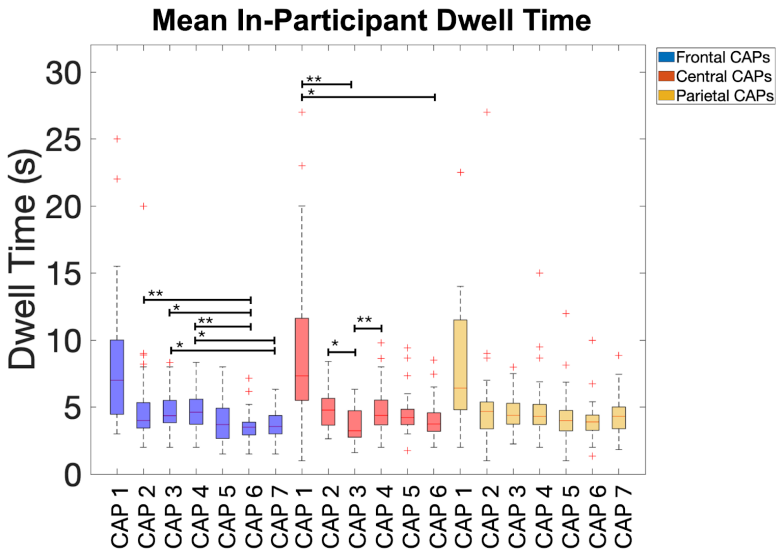

Figure 7. Average in-participant co-activation pattern (CAP) dwell times for all regions of interest. Bracketed pairs show significant statistical differences from Wilcoxon pairwise analysis. Bonferroni corrected: * $p < 0.05$; ** $p < 0.01$; *** $p < 0.001$; **** $p < 0.0001$.

Figure 8 presents the CAP transition probability matrices for frontal, central, and parietal regions. These matrices primarily demonstrate that the most probable transition is between frames of the same CAP, indicating most adjacent frames share membership. This was expected as fluctuations in concentration of oxygenated and deoxygenated hemoglobin are slow, so most adjacent frames will have similar spatial patterns and therefore will likely be grouped into the same CAP cluster. Notably, these matrices are not symmetric along the diagonal.

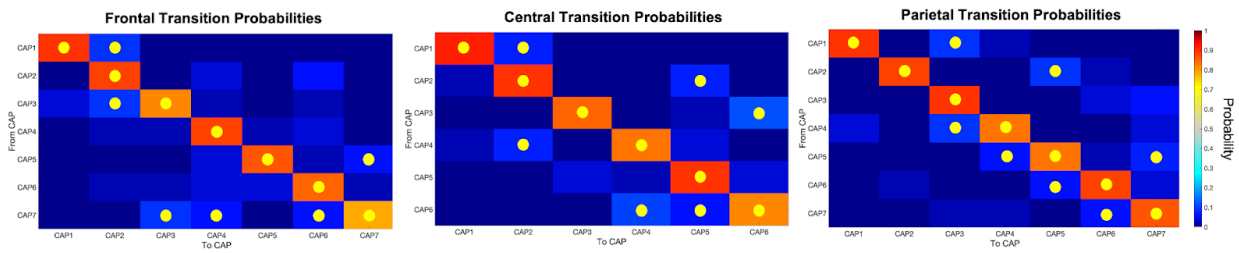

Figure 8. In-participant likelihood of transitioning to a given co-activation pattern (CAP) from each CAP for frontal, central, and parietal regions. Probabilities ≥ 5% are marked with a yellow circle.

4.0 Discussion

4.1 Neonate Functional Connectivity Networks and Co-Activation Patterns (CAPs)

4.1.1 CAP Identification

To the best of our knowledge, this is the first presentation of CAPs derived from neonatal brain activity, marking the first adaptation of the CAP analysis procedure proposed by Liu and Duyn for HD-DOT neonatal data (Liu & Duyn, 2013b). Our primary goal was to establish the feasibility and demonstrate the suitability of HD-DOT data for CAP analysis, particularly in application to newborn infants. Before CAP clustering, we first confirmed that frames with high seed activity were highly correlated with seed-based connectivity maps. This confirmation was critical, as CAP analysis relies on the assumption that top seed-selected frames are a sufficient proxy for seed connectivity. Verifying this assumption with HD-DOT data establishes that CAP analysis is feasible in this context and produces meaningful measures of functional connectivity. The success of the clustering process itself, achieving mean consistency scores exceeding fMRI benchmarks set by Liu and Duyn, further demonstrates the compatibility of HD-DOT with CAP analysis. While HD-DOT's lower spatial coverage compared to fMRI may partially explain this improvement (fewer nodes reduce dimensionality and improve clustering consistency), it nonetheless adds validity to the CAP clusters derived from HD-DOT frames.

4.1.2 CAP Spatial Maps

Establishing the presence of these recurring patterns is significant, as it indicates that traditional neonatal static seed correlation maps may be driven by instantaneous whole-brain co-activation patterns, congruent with adult fMRI CAP studies (Liu & Duyn, 2013b). CAPs present primarily symmetric activity across the left/right hemispheres. Visual inspection reveals some general trends true of each regional CAP set. First, all CAP sets include at least one CAP that corresponds to the seed correlation map (e.g., frontal CAPs 2 and 7, central CAPs 2 and 6, parietal CAP 7). The main differentiating feature of CAPs with similar overall patterns appears to be the magnitude of the activity changes and which sub-regional areas are recruited. For example, frontal CAP 7 appears to be limited to prefrontal activity whereas frontal CAP 2 extends to dorsolateral prefrontal activity. Second, CAP sets typically include an anti-correlation pattern, with positive Δ[HbO] in the seed region paired with negative Δ[HbO] outside the seed region (e.g., frontal CAP 5, central CAP 3, central CAP 5, and parietal CAP 6). Third, all CAP sets have a pattern with global positive Δ[HbO] (e.g., frontal CAP 1, central CAP 1, and parietal CAP 1). While not directly comparable, a neonate fMRI study that looks at patterns of synchronicity rather than patterns of activation, also reports states of global synchronicity (França et al., 2024). Though non-neuronal physiological confounds like respiration are removed during data preprocessing, global fluctuations in hemodynamic activity may still be present, and these CAPs are potentially derived from instances of overall increases of oxygenation in the brain. In the formation of these CAPs, it is possible that a singular high activity pattern does not emerge (instead presenting as globally increased activity), as this CAP is an average of various high-activity patterns. Global signal regression (GSR) was not used in the original analysis because GSR may potentially introduce spurious anti-correlations (Anderson et al., 2011; Murphy & Fox, 2017)), although a similar approach was implemented by regressing out the mean signal from short distance channels. Previous fMRI CAP studies show mixed results on whether GSR has a constructive effect on the patterns that emerge (Liu & Duyn, 2013a, 2013b). To explore the effect of GSR on our data, analysis was repeated with the addition of GSR post preprocessing and before data normalization. The resulting CAPs are documented in the supplemental material (see Supplemental Figure 6). Notably, the global high activity CAPs are no longer present, and anti-correlation is prominent in all patterns. While this study does not focus on the GSR results, as short separation regression sufficiently attenuates physiological confounds and there is little consensus on the use of GSR, future studies may consider using GSR to investigate the impact of global hemodynamic fluctuations on the analysis of co-activation patterns analysis.

Our findings complement the existing literature on neonatal functional connectivity networks. The traditional static analysis (group-level seed correlation activity maps, see Figure 3 and Supplementary Figure 2) closely resembles patterns reported in other neonatal studies describing static functional connectivity (Fransson et al., 2007; Gao et al., 2017; Keunen et al., 2017; Smyser et al., 2010): the frontal activity resembles salience network activity which has been observed in one-month-old participants (Gao et al., 2017); the central activity aligns with descriptions of the sensorimotor network dating back to the first preterm infant resting-state functional connectivity (Fransson et al., 2007); the parietal activity is consistent with descriptions of modular and immature frontoparietal networks (FPNs) and default mode network (DMN), the latter being observed in neonates as young as 29 weeks postmenstrual age (Doria et al., 2010; Gao et al., 2017).

The dynamic decomposition of the parietal regional activity is particularly interesting because it may shed light on early DMN or FPN activity that static approaches are not sensitive to. While the static seed-based correlation maps do not reveal this, the dynamic CAP approach identifies several patterns featuring frontoparietal activity (see Figure 5). Parietal CAPs 3, 4, 7 and frontal CAP 4 illustrate instances where the frontal region and parietal region are co-activated. Parietal CAP 5 highlights an instance of parietal activation paired with weaker frontal activation and prefrontal deactivation. Some of these examples do not show solely frontoparietal activity, but additional selective recruitment of the central region (e.g. parietal CAP 3 and 4). These maps are of great interest, as the DMN and FPN are thought to be immature and modular at this stage in life. An fMRI study of static functional connectivity in 1-month-olds illustrates both the DMN and FPNs as primarily consisting of parietal activity, with little to no recruitment of the frontal region even by 3-months (Gao et al., 2017). Our dynamic functional connectivity analysis suggests these frontoparietal connections are present at birth and that early features of higher-order networks, like the DMN and FPNs, are more time-resolved in neonates. These results corroborate two neonate fMRI studies that found similar frontoparietal patterns using different methods to extract dynamic functional connectivity (França et al., 2024; Ma et al., 2020). Further investigation of these transient frontoparietal patterns may reveal how they influence or contribute to the development of the DMN and FPNs.

While the developmental trajectory of the DMN and FPNs remains an area of ongoing research, this study highlights the merits of examining networks from a dynamic perspective. Only through dynamic decomposition are frontoparietal patterns revealed. These patterns may drive or reflect mechanisms underlying the network's evolution from the immature fragmented neonatal DMN to the mature adult configuration.

4.1.3 CAP Metrics

The metrics used to describe CAPs in this study (consistency, fractional occupancy, dwell time, and transition likelihood) were selected based on previous dynamic functional connectivity studies (Brown & Gartstein, 2023; França et al., 2024; Khan et al., 2022; Liu et al., 2018). The CAPs with global positive Δ[HbO] demonstrated the highest intra-cluster consistency within each set. We hypothesize that this is likely due to these CAPs' relatively simple spatial pattern, which minimizes variability across participants. CAPs with lower consistency scores may reflect the presence of outlier frames (frames which do not resemble any particular recurring pattern). Future studies may consider formulating a method to exclude these outliers before clustering, as it may improve CAP consistency scores.

Fractional occupancy of the global positive Δ[HbO] CAPs appears to be significantly lower than several other CAPs within each region. CAPs with significantly lower fractional occupancies also tend to contain the most negative Δ[HbO] patterns (frontal CAP 5, central CAP 3, and parietal CAP 2). While CAP mean dwell time was around 3-5 seconds, the global positive Δ[HbO] CAP frequently displayed a wider spread of higher dwell times, though this difference was only significant in the central region for two central CAPs. The transition likelihood matrices

characterize how CAPs are related to one another. Although this study did not assess the statistical significance of specific transitions due to the large number of comparisons and lack of a clear hypothesis, visual inspection suggests relevant trends that warrant further investigation in future research. The transition matrices are dominated by reflexive transitions, indicating frames of one CAP most often transition to frames of the same CAP. Still, CAPs appear to be more associated with some CAPs (usually just one) when compared with others, showing CAPs are not equally related. Notably, these matrices are not symmetric along the diagonal. This suggests that if CAPs are weakly associated, they may be related in a non-reciprocal manner.

4.2 Addressing Challenges in Neonatal Imaging

CAP analysis paired with HD-DOT offers significant advantages for functional imaging brain studies in neonates and is a promising avenue for future dynamic functional connectivity studies. As previous studies (Collins-Jones et al., 2024; Frijia et al., 2021; Uchitel et al., 2023) have established, HD-DOT is particularly fit for imaging the infant cortex, as infant brains are smaller and their skulls are thinner than those of adults, allowing the NIR light to penetrate more deeply. These studies highlight that the LUMO system is comfortable, wearable, partially motion-tolerant, and non-invasive, qualities that can enable longer and more naturalistic studies of infants (Collins-Jones et al., 2024; Frijia et al., 2021; Uchitel et al., 2023). This study validates an analysis method, CAP analysis, which can complement HD-DOT's strengths because it is also resilient to challenges in neonatal brain imaging analysis. Unlike other methods that rely on long, continuous datasets (e.g., correlation, ICA, dynamic ICA), CAP analysis is effective even when limited to shorter or discontinuous data segments. This is a significant advantage, as neonatal datasets are often hindered by motion artifacts and interruptions due to infant non-compliance. By focusing on singular high-activity frames, CAP analysis bypasses the typical dependency on long data windows, making it an ideal tool for studying the infant brain.

Though this study focused on healthy term infants, HD-DOT is also suitable for imaging sick or preterm infants in neonatal intensive care. Methods capable of studying these vulnerable populations is a crucial prerequisite to monitoring and improving their clinical outcomes.

4.3 Limitations

4.3.1 Recruiting

As with most neonatal studies, data collection was limited due to inherent difficulties recruiting and studying newborn infants. Studies were conducted opportunistically cot-side in between feeds, so data collection was sometimes interrupted by unavoidable circumstances such as the baby waking and needing consoling, the family having visitors, or the family discharging from the hospital. Additionally, some infants naturally startled or fidgeted more than others, resulting in data loss. Compared to fMRI and EEG, HD-DOT is more resistant to motion, but it is still sensitive to gross movements, resulting in data loss.

4.3.2 HD-DOT cap coverage

This study targeted particular regions to test HD-DOT CAP analysis in neonates. The LUMO caps were designed to specifically target these areas. Future studies may consider using a HD-DOT montage with whole-head coverage to examine other regions and networks of interest, particularly the occipital region/visual network and temporal region/auditory network, which we were not able to assess in this study.

4.3.3 Selecting k

Though k selection is empirically chosen and data-driven in this study, it was apparent during analysis that silhouette score is not an ideal metric to use in k selection due to the nature of brain data. Silhouette score is not only a measure of intra-cluster similarity but also inter-cluster separation. Even after processing with PCA, it is unclear whether we can reasonably expect well-separated clusters in spatial brain data, as states may be highly similar spatially but differ functionally. Even though we arrive at a compelling optimal k using silhouette scores and the elbow method, the silhouette scores themselves appear to be low. Since consistency, a measure of intra-cluster similarity, is high, we hypothesize that the silhouette scores are low because of poor cluster separation. Liu addresses a similar concern in their paper (Liu et al., 2018), hypothesizing that activity patterns do not need to be distinct in order to be meaningful. We agree that our results are hierarchical groupings of frames rather than clearly disparate clusters. Nevertheless, k selection is non-trivial, as choosing too high a k increases redundancy of CAPs and choosing too low a k washes out potential nuances by combining clusters that should be distinct. Selecting a data-driven k optimizes these two opposing risks. We use CAP consistency to determine whether a pattern in the dataset is reliable. Thus, even if silhouette scores are low, sufficient consistency allows us to be confident in our clusters.

4.3.4 Methodological Standardization

Given that HD-DOT CAP neonate research is still in early development, the field lacks consensus for several steps in the preprocessing and postprocessing pipeline, including data cleaning, seed selection, and defining data quality thresholds. Though this work references previous HD-DOT infant studies for hyperparameters during preprocessing, a few novel decisions were made which would benefit from standardization in the future. One example is that this study pilots data-driven seed selection done at the participant level. This study aims to establish a strong case for CAP analysis with HD-DOT, and its success underscores the need for further methodological standardization to enhance reproducibility and comparability across studies.

5.0 Conclusion

This study offers a novel perspective on neonatal brain activity, marking the first application of CAP analysis in neonatal HD-DOT data. Our findings not only confirm the suitability of CAP analysis for neonatal HD-DOT data but contribute valuable dynamic representations of known resting-state networks early in life. Future work involving larger longitudinal datasets may reveal how resting-state dynamic functional connectivity evolves over time. Through understanding the developmental trajectory of functional networks, we will enhance our understanding of typical and atypical brain development in early infancy.

References

Adhikari, M. H., Belloy, M. E., Van der Linden, A., Keliris, G. A., & Verhoye, M. (2021). Resting-State Co-activation Patterns as Promising Candidates for Prediction of Alzheimer's Disease in Aged Mice. *Frontiers in Neural Circuits*, *14*. https://doi.org/10.3389/fncir.2020.612529

Alexander, B., Loh, W. Y., Matthews, L. G., Murray, A. L., Adamson, C., Beare, R., Chen, J., Kelly, C. E., Anderson, P. J., Doyle, L. W., Spittle, A. J., Cheong, J. L. Y., Seal, M. L., & Thompson, D. K. (2019). Desikan-Killiany-Tourville Atlas Compatible Version of M-CRIB Neonatal Parcellated Whole Brain Atlas: The M-CRIB 2.0. *Frontiers in Neuroscience*, *13*, 34. https://doi.org/10.3389/fnins.2019.00034

Anderson, J. S., Druzgal, T. J., Lopez-Larson, M., Jeong, E., Desai, K., & Yurgelun-Todd, D. (2011). Network anticorrelations, global regression, and phase-shifted soft tissue correction. *Human Brain Mapping*, *32*(6), 919–934. https://doi.org/10.1002/hbm.21079

Arimitsu, T., Shinohara, N., Minagawa, Y., Hoshino, E., Hata, M., & Takahashi, T. (2022). Differential age-dependent development of inter-area brain connectivity in term and preterm neonates. *Pediatric Research*, *92*(4), 1017–1025. https://doi.org/10.1038/s41390-022-01939-7

Arridge, S. R. (1999). Optical tomography in medical imaging. *Inverse Problems*, *15*(2), R41–R93. https://doi.org/10.1088/0266-5611/15/2/022

Arridge, S. R., & Schotland, J. C. (2009). Optical tomography: Forward and inverse problems. *Inverse Problems*, *25*(12), 123010. https://doi.org/10.1088/0266-5611/25/12/123010

Arthurs, O. J., Edwards, A., Austin, T., Graves, M. J., & Lomas, D. J. (2012). The challenges of neonatal magnetic resonance imaging. *Pediatric Radiology*, *42*(10), 1183–1194. https://doi.org/10.1007/s00247-012-2430-2

Blanco, B., Molnar, M., Carreiras, M., Collins-Jones, L. H., Vidal, E., Cooper, R. J., & Caballero-Gaudes, C. (2021). Group-level cortical functional connectivity patterns using fNIRS: Assessing the effect of bilingualism in young infants. *Neurophotonics*, *8*(2), 025011. https://doi.org/10.1117/1.NPh.8.2.025011

Brown, K. L., & Gartstein, M. A. (2023). Microstate analysis in infancy. *Infant Behavior and Development*, *70*, 101785. https://doi.org/10.1016/j.infbeh.2022.101785

Cabral, J., Vidaurre, D., Marques, P., Magalhães, R., Silva Moreira, P., Miguel Soares, J., Deco, G., Sousa, N., & Kringelbach, M. L. (2017). Cognitive performance in healthy older adults relates to spontaneous switching between states of functional connectivity during rest. *Scientific Reports*, *7*(1), 5135. https://doi.org/10.1038/s41598-017-05425-7

Collins-Jones, L. H., Arichi, T., Poppe, T., Billing, A., Xiao, J., Fabrizi, L., Brigadoi, S., Hebden, J. C., Elwell, C. E., & Cooper, R. J. (2021). Construction and validation of a database of head models for functional imaging of the neonatal brain. *Human Brain Mapping*, *42*(3), 567–586. https://doi.org/10.1002/hbm.25242

Collins-Jones, L. H., Gossé, L. K., Blanco, B., Bulgarelli, C., Siddiqui, M., Vidal-Rosas, E. E., Duobaitė, N., Nixon-Hill, R. W., Smith, G., Skipper, J., Sargent, T., Powell, S., Everdell, N. L., Jones, E. J. H., & Cooper, R. J. (2024). Whole-head high-density diffuse optical tomography to map infant audio-visual responses to social and non-social stimuli. *Imaging Neuroscience*, *2*, 1–19. https://doi.org/10.1162/imag_a_00244

Deen, B., Richardson, H., Dilks, D. D., Takahashi, A., Keil, B., Wald, L. L., Kanwisher, N., & Saxe, R. (2017).

Organization of high-level visual cortex in human infants. *Nature Communications*, *8*(1), 13995. https://doi.org/10.1038/ncomms13995

Doria, V., Beckmann, C. F., Arichi, T., Merchant, N., Groppo, M., Turkheimer, F. E., Counsell, S. J., Murgasova, M., Aljabar, P., Nunes, R. G., Larkman, D. J., Rees, G., & Edwards, A. D. (2010). Emergence of resting state networks in the preterm human brain. *Proceedings of the National Academy of Sciences*, *107*(46), 20015–20020. https://doi.org/10.1073/pnas.1007921107

Edwards, A. D., Rueckert, D., Smith, S. M., Abo Seada, S., Alansary, A., Almalbis, J., Allsop, J., Andersson, J., Arichi, T., Arulkumaran, S., Bastiani, M., Batalle, D., Baxter, L., Bozek, J., Braithwaite, E., Brandon, J., Carney, O., Chew, A., Christiaens, D., … Hajnal, J. V. (2022). The Developing Human Connectome Project Neonatal Data Release. *Frontiers in Neuroscience*, *16*, 886772. https://doi.org/10.3389/fnins.2022.886772

Eyre, M., Fitzgibbon, S. P., Ciarrusta, J., Cordero-Grande, L., Price, A. N., Poppe, T., Schuh, A., Hughes, E., O'Keeffe, C., Brandon, J., Cromb, D., Vecchiato, K., Andersson, J., Duff, E. P., Counsell, S. J., Smith, S. M., Rueckert, D., Hajnal, J. V., Arichi, T., … Edwards, A. D. (2021). The Developing Human Connectome Project: Typical and disrupted perinatal functional connectivity. *Brain*, *144*(7), 2199–2213. https://doi.org/10.1093/brain/awab118

França, L. G. S., Ciarrusta, J., Gale-Grant, O., Fenn-Moltu, S., Fitzgibbon, S., Chew, A., Falconer, S., Dimitrova, R., Cordero-Grande, L., Price, A. N., Hughes, E., O'Muircheartaigh, J., Duff, E., Tuulari, J. J., Deco, G., Counsell, S. J., Hajnal, J. V., Nosarti, C., Arichi, T., … Batalle, D. (2024). Neonatal brain dynamic functional connectivity in term and preterm infants and its association with early childhood neurodevelopment. *Nature Communications*, *15*(1), 16. https://doi.org/10.1038/s41467-023-44050-z

Fransson, P., Skiöld, B., Horsch, S., Nordell, A., Blennow, M., Lagercrantz, H., & Åden, U. (2007). Resting-state networks in the infant brain. *Proceedings of the National Academy of Sciences*, *104*(39), 15531–15536. https://doi.org/10.1073/pnas.0704380104

Frijia, E. M., Billing, A., Lloyd-Fox, S., Vidal Rosas, E., Collins-Jones, L., Crespo-Llado, M. M., Amadó, M. P., Austin, T., Edwards, A., Dunne, L., Smith, G., Nixon-Hill, R., Powell, S., Everdell, N. L., & Cooper, R. J. (2021). Functional imaging of the developing brain with wearable high-density diffuse optical tomography: A new benchmark for infant neuroimaging outside the scanner environment. *NeuroImage*, *225*, 117490. https://doi.org/10.1016/j.neuroimage.2020.117490

Gao, W., Lin, W., Grewen, K., & Gilmore, J. H. (2017). Functional Connectivity of the Infant Human Brain. *The Neuroscientist*.

Gemma, M., de Vitis, A., Baldoli, C., Calvi, M. R., Blasi, V., Scola, E., Nobile, L., Iadanza, A., Scotti, G., & Beretta, L. (2009). Functional magnetic resonance imaging (fMRI) in children sedated with propofol or midazolam. *Journal of Neurosurgical Anesthesiology*, *21*(3), 253–258. https://doi.org/10.1097/ANA.0b013e3181a7181d

Hassanzadeh, E., Hornak, A., Hassanzadeh, M., Warfield, S. K., Pearl, P. L., Bolton, J., Suarez, R., Stone, S., Stufflebeam, S., & Ailion, A. S. (2023). Comparison of fMRI language laterality with and without sedation in pediatric epilepsy. *NeuroImage : Clinical*, *38*, 103448. https://doi.org/10.1016/j.nicl.2023.103448

Hermans, T., Khazaei, M., Raeisi, K., Croce, P., Tamburro, G., Dereymaeker, A., De Vos, M., Zappasodi, F., & Comani, S. (2023). Microstate Analysis Reflects Maturation of the Preterm Brain. *Brain Topography*. https://doi.org/10.1007/s10548-023-01008-0

Huppert, T. J., Diamond, S. G., Franceschini, M. A., & Boas, D. A. (2009). HomER: A review of time-series analysis methods for near-infrared spectroscopy of the brain. *Applied Optics*, *48*(10), D280–D298. https://doi.org/10.1364/AO.48.00D280

Hutchison, R. M., Womelsdorf, T., Allen, E. A., Bandettini, P. A., Calhoun, V. D., Corbetta, M., Della Penna, S., Duyn, J. H., Glover, G. H., Gonzalez-Castillo, J., Handwerker, D. A., Keilholz, S., Kiviniemi, V., Leopold, D. A., De Pasquale, F., Sporns, O., Walter, M., & Chang, C. (2013). Dynamic functional connectivity: Promise, issues, and interpretations. *NeuroImage*, *80*, 360–378. https://doi.org/10.1016/j.neuroimage.2013.05.079

Jones, D. T., Vemuri, P., Murphy, M. C., Gunter, J. L., Senjem, M. L., Machulda, M. M., Przybelski, S. A., Gregg, B. E., Kantarci, K., Knopman, D. S., Boeve, B. F., Petersen, R. C., & Jr, C. R. J. (2012). Non-Stationarity in the "Resting Brain's" Modular Architecture. *PLOS ONE*, *7*(6), e39731. https://doi.org/10.1371/journal.pone.0039731

Keunen, K., Counsell, S. J., & Benders, M. J. N. L. (2017). The emergence of functional architecture during early brain development. *NeuroImage*, *160*, 2–14. https://doi.org/10.1016/j.neuroimage.2017.01.047

Khan, A. F., Zhang, F., Shou, G., Yuan, H., & Ding, L. (2022). Transient brain-wide coactivations and structured transitions revealed in hemodynamic imaging data. *NeuroImage*, *260*, 119460. https://doi.org/10.1016/j.neuroimage.2022.119460

Lee, C. W., Cooper, R. J., & Austin, T. (2017). Diffuse optical tomography to investigate the newborn brain. *Pediatric Research*, *82*(3), 376–386. https://doi.org/10.1038/pr.2017.107

Lee, M. H., Smyser, C. D., & Shimony, J. S. (2013). Resting-State fMRI: A Review of Methods and Clinical Applications. *American Journal of Neuroradiology*, *34*(10), 1866–1872. https://doi.org/10.3174/ajnr.A3263

Liu, X., & Duyn, J. (2013a). Resting-State fMRI Signal Anti-Correlation Exists in Absence of Global Signal Regression. *21st ISMRM Annu. Meet. 2251. Salt Lake City, Utah, USA.*

Liu, X., & Duyn, J. H. (2013b). Time-varying functional network information extracted from brief instances of spontaneous brain activity. *Proceedings of the National Academy of Sciences*, *110*(11), 4392–4397. https://doi.org/10.1073/pnas.1216856110

Liu, X., Zhang, N., Chang, C., & Duyn, J. H. (2018). Co-activation patterns in resting-state fMRI signals. *NeuroImage*, *180*, 485–494. https://doi.org/10.1016/j.neuroimage.2018.01.041

López-Vicente, M., Agcaoglu, O., Pérez-Crespo, L., Estévez-López, F., Heredia-Genestar, J. M., Mulder, R. H., Flournoy, J. C., Van Duijvenvoorde, A. C. K., Güroğlu, B., White, T., Calhoun, V., Tiemeier, H., & Muetzel, R. L. (2021). Developmental Changes in Dynamic Functional Connectivity From Childhood Into Adolescence. *Frontiers in Systems Neuroscience*, *15*, 724805. https://doi.org/10.3389/fnsys.2021.724805

Ma, X., Wu, X., & Shi, Y. (2020). Changes of Dynamic Functional Connectivity Associated With Maturity in Late Preterm Infants. *Frontiers in Pediatrics*, *8*, 412. https://doi.org/10.3389/fped.2020.00412

Marshall, E., Nomi, J. S., Dirks, B., Romero, C., Kupis, L., Chang, C., & Uddin, L. Q. (2020). Coactivation pattern analysis reveals altered salience network dynamics in children with autism spectrum disorder. *Network Neuroscience*, *4*(4), 1219–1234. https://doi.org/10.1162/netn_a_00163

Marusak, H. A., Calhoun, V. D., Brown, S., Crespo, L. M., Sala-Hamrick, K., Gotlib, I. H., & Thomason, M. E. (2017). Dynamic functional connectivity of neurocognitive networks in children. *Human Brain Mapping*, *38*(1), 97–108. https://doi.org/10.1002/hbm.23346

Mawla, I., Huang, Z., Kaplan, C. M., Ichesco, E., Waller, N., Larkin, T. E., Zöllner, H. J., Edden, R. A. E., Harte, S. E., Clauw, D. J., Mashour, G. A., Napadow, V., & Harris, R. E. (2023). Large-scale momentary brain co-activation patterns are associated with hyperalgesia and mediate focal neurochemistry and cross-network functional connectivity in fibromyalgia. *Pain*, *164*(12), 2737–2748. https://doi.org/10.1097/j.pain.0000000000002973

Menon, V. (2013). Developmental pathways to functional brain networks: Emerging principles. *Trends in Cognitive Sciences*, *17*(12), 627–640. https://doi.org/10.1016/j.tics.2013.09.015

Mohammadi-Nejad, A.-R., Mahmoudzadeh, M., Hassanpour, M. S., Wallois, F., Muzik, O., Papadelis, C., Hansen, A., Soltanian-Zadeh, H., Gelovani, J., & Nasiriavanaki, M. (2018). Neonatal brain resting-state functional connectivity imaging modalities. *Photoacoustics*, *10*, 1–19. https://doi.org/10.1016/j.pacs.2018.01.003

Murphy, K., & Fox, M. D. (2017). Towards a consensus regarding global signal regression for resting state functional connectivity MRI. *NeuroImage*, *154*, 169–173. https://doi.org/10.1016/j.neuroimage.2016.11.052

Niu, W., Xu, X., Zhang, H., Zhang, Y., Ni, S., Liu, T., Li, Q., Lai, C., & Sun, Y. (2020). Breastfeeding improves dynamic reorganization of functional connectivity in preterm infants: A temporal brain network study. *Medical & Biological Engineering & Computing*, *58*(11), 2805–2819. https://doi.org/10.1007/s11517-020-02244-3

Pedregosa, F., Varoquaux, G., Gramfort, A., & Michel, V. (2011). Scikit-learn: Machine Learning in Python. *Journal of Machine Learning Research*, *12*, 2825–2830.

Peng, C., & Hou, X. (2021). Applications of functional near-infrared spectroscopy (fNIRS) in neonates. *Neuroscience Research*, *170*, 18–23. https://doi.org/10.1016/j.neures.2020.11.003

Power, J. D., Fair, D. A., Schlaggar, B. L., & Petersen, S. E. (2010). The Development of Human Functional Brain Networks. *Neuron*, *67*(5), 735–748. https://doi.org/10.1016/j.neuron.2010.08.017

Preti, M. G., Bolton, T. A., & Van De Ville, D. (2017). The dynamic functional connectome: State-of-the-art and perspectives. *NeuroImage*, *160*, 41–54. https://doi.org/10.1016/j.neuroimage.2016.12.061

Qin, J., Chen, S.-G., Hu, D., Zeng, L.-L., Fan, Y.-M., Chen, X.-P., & Shen, H. (2015). Predicting individual brain maturity using dynamic functional connectivity. *Frontiers in Human Neuroscience*, *9*. https://doi.org/10.3389/fnhum.2015.00418

R Core Team. (2017). *R: A language and environment for statistical computing.* [Computer software]. R Foundation for Statistical Computing. http://www.R-project.org/

Ren, H., Jiang, X., Meng, L., Lu, C., Wang, L., Dai, C., & Chen, W. (2022). fNIRS-Based Dynamic Functional

Connectivity Reveals the Innate Musical Sensing Brain Networks in Preterm Infants. *IEEE Transactions on Neural Systems and Rehabilitation Engineering*, *30*, 1806–1816. https://doi.org/10.1109/TNSRE.2022.3178078

Sato, T., Nambu, I., Takeda, K., Aihara, T., Yamashita, O., Isogaya, Y., Inoue, Y., Otaka, Y., Wada, Y., Kawato, M., Sato, M., & Osu, R. (2016). Reduction of global interference of scalp-hemodynamics in functional near-infrared spectroscopy using short distance probes. *NeuroImage*, *141*, 120–132. https://doi.org/10.1016/j.neuroimage.2016.06.054

Schweiger, M., & Arridge, S. (2014). The Toast++ software suite for forward and inverse modeling in optical tomography. *Journal of Biomedical Optics*, *19*(4), 040801. https://doi.org/10.1117/1.JBO.19.4.040801

Shen, H., Li, Z., Zeng, L.-L., Yuan, L., Chen, F., Liu, Z., & Hu, D. (2014). Internetwork dynamic connectivity effectively differentiates schizophrenic patients from healthy controls. *NeuroReport*, *25*(17), 1344. https://doi.org/10.1097/WNR.0000000000000267

Smyser, C. D., Inder, T. E., Shimony, J. S., Hill, J. E., Degnan, A. J., Snyder, A. Z., & Neil, J. J. (2010). Longitudinal Analysis of Neural Network Development in Preterm Infants. *Cerebral Cortex*, *20*(12), 2852–2862. https://doi.org/10.1093/cercor/bhq035

Stoecklein, S., Hilgendorff, A., Li, M., Förster, K., Flemmer, A. W., Galiè, F., Wunderlich, S., Wang, D., Stein, S., Ehrhardt, H., Dietrich, O., Zou, Q., Zhou, S., Ertl-Wagner, B., & Liu, H. (2020). Variable functional connectivity architecture of the preterm human brain: Impact of developmental cortical expansion and maturation. *Proceedings of the National Academy of Sciences*, *117*(2), 1201–1206. https://doi.org/10.1073/pnas.1907892117

Uchitel, J., Blanco, B., Collins-Jones, L., Edwards, A., Porter, E., Pammenter, K., Hebden, J., Cooper, R. J., & Austin, T. (2023). Cot-side imaging of functional connectivity in the developing brain during sleep using wearable high-density diffuse optical tomography. *NeuroImage*, *265*, 119784. https://doi.org/10.1016/j.neuroimage.2022.119784

Wang, J., Li, H., Cecil, K. M., Altaye, M., Parikh, N. A., & He, L. (2024). DFC-Igloo: A dynamic functional connectome learning framework for identifying neurodevelopmental biomarkers in very preterm infants. *Computer Methods and Programs in Biomedicine*, *257*, 108479. https://doi.org/10.1016/j.cmpb.2024.108479

Wen, X., Wang, R., Yin, W., Lin, W., Zhang, H., & Shen, D. (2020). Development of Dynamic Functional Architecture during Early Infancy. *Cerebral Cortex*, *30*(11), 5626–5638. https://doi.org/10.1093/cercor/bhaa128

Yang, H., Zhang, H., Di, X., Wang, S., Meng, C., Tian, L., & Biswal, B. (2021). *Reproducible Coactivation Patterns of Functional Brain Networks Reveal the Aberrant Dynamic State Transition in Schizophrenia* (p. 2021.03.29.437611). bioRxiv. https://doi.org/10.1101/2021.03.29.437611

Yang, J., Gohel, S., & Vachha, B. (2020). Current methods and new directions in resting state fMRI. *Clinical Imaging*, *65*, 47–53. https://doi.org/10.1016/j.clinimag.2020.04.004

Yin, W., Li, T., Hung, S.-C., Zhang, H., Wang, L., Shen, D., Zhu, H., Mucha, P. J., Cohen, J. R., & Lin, W. (2020).

The emergence of a functionally flexible brain during early infancy. *Proceedings of the National Academy of Sciences*, *117*(38), 23904–23913. https://doi.org/10.1073/pnas.2002645117

Yücel, M. A., Lühmann, A. V., Scholkmann, F., Gervain, J., Dan, I., Ayaz, H., Boas, D., Cooper, R. J., Culver, J., Elwell, C. E., Eggebrecht, A., Franceschini, M. A., Grova, C., Homae, F., Lesage, F., Obrig, H., Tachtsidis, I., Tak, S., Tong, Y., … Wolf, M. (2021). Best practices for fNIRS publications. *Neurophotonics*, *8*(01). https://doi.org/10.1117/1.NPh.8.1.012101